International Journal of Thermofluid Science and Technology (2022)
Volume 9, Issue 1, Paper No. 090105
https://doi.org/10.36963/IJTST.2022090105
Research Article

Numerical Aerodynamic Analysis of a Reflexed Airfoil, N60R, in Ground Effect with Regression Models

Mongkol Thianwiboon

Faculty of Engineering, Mahidol University, Nakorn Pathom 73170, Thailand

ARTICLE INFO

Received: 20 Aug. 2021;
Received in revised form:
02 Nov. 2021;
Accepted: 08 Nov. 2021;
Published online:
15 Nov. 2021

Keywords:
Wing-in-ground effect craft
WIG
Ground effect
N60R
CFD

ABSTRACT

Flight in the vicinity of the ground is known to be more efficient than flight in a free air stream. However, a nose-down pitching moment created by a typical cambered airfoil generally increases due to ground effect. Thus, a larger tail for the aircraft is required to remain stable, which creates more drag and reduces the efficiency. The pitching moment in the ground effect becomes more complicated because it varies with height above the ground. Thus, the reflexed or S-shaped airfoil was introduced to overcome this effect. The addition of reflex reduces the lift of the airfoil, but it is required for improved stability.

This study applied computational fluid dynamics to investigate the aerodynamic characteristics of a reflexed airfoil, N60R, in ground effect over a range of angles of attack from 0° to 20° at a Reynolds number from 0.8×10^6 to 5×10^6 and ground clearance from 5% to 150% of the chord. The numerical results reveal that the boundary layer close to the ground affects the lift, drag, pitching moment coefficients, and center of pressure.

As the airfoil operates close to the ground, the lift increased due to a higher pressure build up under the airfoil. Except for a relatively low angle of attack (less than 2°), the lift decreases with a reduction in ground clearance due to loss of upper surface suction. The maximum lift-to-drag ratio, approximately 120, occurred at an angle of attack of 6° and ground clearance of 5%.

In summary, this study presents the aerodynamic characteristics of the reflexed airfoil, N60R, over a wide range of angles of attack, Reynolds numbers and ground clearance. Furthermore, regression models for each characteristic were developed and can be used to predict the coefficients of the N60R without the need for consuming time in Computational Fluid Dynamics (CFD) analysis.

*Corresponding e-mail: mongkol.thi@mahidol.ac.th (Mongkol Thianwiboon)

Nomenclature

c	chord length
C_d	drag coefficient
C_l	lift coefficient
C_m	pitching moment coefficient (at 0.25c)
h_t	distance of the trailing edge above the ground
h_c	ground clearance ratio (h_t /c)
Ma	Mach number
Re	Reynolds number
U	free stream velocity
X_{cp}	center of pressure (percent of chord from the leading edge)
k	turbulent kinetic energy
u_i	velocity components (i = 1, 2, 3)
R^2	coefficient of determination

Greek symbols

α	angle of attack
ε	turbulent dissipation energy
ω	specific dissipation rate
μ	dynamic viscosity
μ_t	turbulent viscosity
ρ	density

Abbreviations

GE	ground effect
SST	shear stress transport
WIG	wing-in-ground effect
RANS	Reynolds Average Navier–Stokes

1. Introduction

The classic paper written by Gabrielli and von Kármán [1] demonstrated the balance of the cost and time value of people and cargo idle in transit. At the center of von Kármán-Gabrielli's diagram, there is a gap which is not covered by conventional maritime, land or aerial vehicles. Since the 1960s, researchers and developers have been working on non-conventional WIG craft to fill this gap in the diagram [2, 3]. To enable WIG craft to cruise faster than marine vessels and be more efficient than airplanes, most research has adapted existing technology to exploit the ground effect [4].

The main parameter in most experimental and numerical studies on various airfoils is the ground clearance (h_c), described as the proportion of the distance of the trailing edge above the ground (h_t) to the chord length (c). Typically, aerodynamic characteristics, such as lift, drag and pitching moment coefficient (C_l, C_d and C_m) were studied. Ranzenbach [5] studied the performance of an inverted NACA 4412 airfoil used as a race car front wing in GE. The results show that significant downforce occurred when the ground clearance (h_c) was roughly equal to 0.04 and maximum at h_c of 0.8. The merging of the wing and ground boundary layers causes the downforce to increase as h_c decreases. The flow around the NACA 4412 airfoil with various ground clearances (h_c) was examined numerically and experimentally with fixed and moving ground conditions [6-8]. The lift coefficient in GE was greater than in the free stream. The lift dropped significantly with small ground clearance (h_c = 0.05) due to suction in the passage between the airfoil and the ground which has a convergent–divergent shape. An extensive wind tunnel test was conducted on NACA 6409 in GE with a fixed ground boundary condition [9]. The results show that, by increasing α with low h_c, the center of pressure (X_{cp}) was shifted toward the leading edge and the lift-to-drag ratio was increased. Various airfoils were investigated in GE using different turbulence models such as the standard k-ε, realizable and SST variants of the k-ω model [3, 10-16].

The previous studies show that some well-known airfoils are used in the WIG, such as NACA 6409, NACA 4412 and Clark-Y. The NACA 6409 is an excellent airfoil at low speed, but its large camber limits its high-speed performance. The NACA 4412 and Clark-Y are recognized for their performance in GE due to the flat bottom since this prevents the negative ground effect produced by a high cambered airfoil [17]. The reflexed airfoil, N60R, with 'S' sections at the trailing edge has better stability compare to the traditional airfoil, thus the horizontal stabilizer area can be reduced at the expense of lift. Small WIG craft tend to utilize the Lippisch planform as

shown in Fig. 1. It is a low aspect ratio reverse delta wing with anhedral angle. It resembles the flying wing [4], which typically uses a reflexed airfoil [18]. Because of the reflexed trailing edge, the change in pitching moment with ground clearance is less noticeable. Thus, the required control power necessary for the transition in height is reduced leading to a reduction in the tail plane area [4, 13]. However, the investigation of the reflexed airfoil is still lacking and limited in the small ranges of α and h_c.

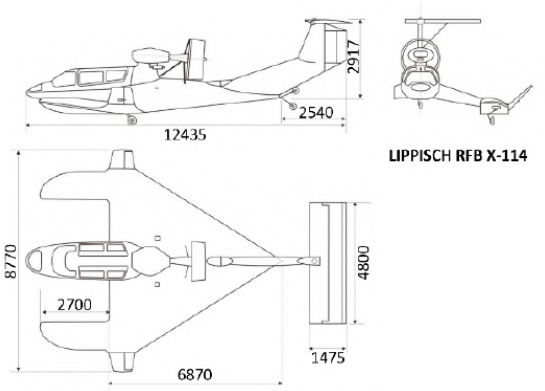

Fig. 1. Example of WIG craft with Lippisch planform

The main objective of the present work is to investigate the aerodynamic characteristics of the N60R with the 'S' sections at the trailing edge in GE. Numerical simulations were conducted with the SST *k-ω* turbulence model at various Reynolds Numbers, angles of attack and ground clearances. Furthermore, regression models for each characteristic were developed and can be used to predict the aerodynamic coefficients of the N60R without the need for time consuming CFD.

2. Governing equations

The RANS equations with SST *k-ω* turbulence model were used to investigate the steady, incompressible flow over the airfoil in ANSYS Fluent 2021 R1. A pressure-based double precision solver with a coupled algorithm for the pressure-velocity coupling was selected. The transport equations of the SST *k-ω* model are expressed below.

$$\frac{\partial}{\partial t}(\rho k) + \frac{\partial}{\partial x_i}(\rho k u_i) = \frac{\partial}{\partial x_j}\left(\Gamma_k \frac{\partial k}{\partial x_j}\right) + G_k - Y_k + S_k \quad (1)$$

$$\frac{\partial}{\partial t}(\rho \omega) + \frac{\partial}{\partial x_j}(\rho \omega u_j) = \frac{\partial}{\partial x_j}\left(\Gamma_\omega \frac{\partial \omega}{\partial x_j}\right) + G_\omega - Y_\omega + D_\omega + S_\omega \quad (2)$$

G_k, G_ω, Y_k and Y_ω are the generation and the dissipation of k and ω respectively. D_ω is the cross-diffusion term. S_k and S_ω are source terms defined by the user. The diffusivity of k and ω defined as Γ_k and Γ_ω are shown below.

$$\Gamma_k = \mu + \frac{\mu_t}{\sigma_k} \quad (3)$$

$$\Gamma_\omega = \mu + \frac{\mu_t}{\sigma_\omega} \quad (4)$$

where the turbulent Prandtl numbers for k and ω are defined as σ_k and σ_ω, respectively. The term G, Y, D, S and μ_t is given in the references [19, 20]. The model boundary conditions are:

$$\frac{U}{L} < \omega_{farfield} < 10\frac{U}{L} \quad (5)$$

$$\frac{10^{-5}U^2}{Re_L} < k_{farfield} < \frac{0.1U^2}{Re_L} \quad (6)$$

$$\omega_{wall} = \frac{6\nu}{\beta_1(\Delta d_1)^2} \quad (7)$$

$$k_{wall} = 0 \quad (8)$$

where L is the approximate length of the computational domain. The lift, drag, pitching moment coefficients and the center of pressure were determined by

$$C_l = \frac{L}{0.5\rho U^2 S} \quad (9)$$

$$C_d = \frac{D}{0.5\rho U^2 S} \quad (10)$$

$$C_m = \frac{M}{0.5\rho U^2 Sc} \quad (11)$$

$$X_{cp} = 0.25 + \frac{C_m}{(C_L cos\alpha + C_D sin\alpha)} \quad (12)$$

3. Validation of the numerical method

3.1 Airfoil geometry

The flow was studied on the N60R airfoil with a reflexed trailing edge. This airfoil is modified from the Navy 60 (N60) airfoil to obtain a pitching moment of zero about the aerodynamic center [21]. Fig. 2 shows the comparison between the N60 and N60R airfoil when the N60R chord is aligned with the horizontal axis.

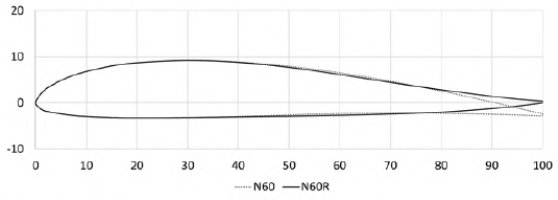

Fig. 2. Geometry of N60 and N60R

3.2 Mesh independence study

Mesh independence studies were carried out by computing the out-of-ground effect flow around the N60R airfoil with chord length (c) = 1 m. The aerodynamic characteristics such as C_l, C_d and C_m were determined at operating temperature 288.16 K, average flow velocity 45 m/s, *Re* of 3×10^6, *Ma* = 0.13 and $\alpha = 6°$ while keeping the density and viscosity of the air at 1.225 kg/m^3 and 1.8375×10^{-5} kg/(m · s), respectively. The turbulent intensity at the velocity inlet is 5% and the turbulent viscosity ratio is 10.

The computational domain and generated mesh for this study are shown in Fig. 3. The upstream and downstream boundaries are defined as the velocity inlet and pressure outlet, respectively. A no-slip condition is defined for the airfoil. A distance of 2c is set from the velocity inlet to the leading edge and the distance from the trailing edge to the pressure outlet is 10c. Both distances from the trailing edge to the upper and lower wall are set to 5c. These distances are set up to confirm they are large enough and have an insignificant effect on the aerodynamics of the airfoil.

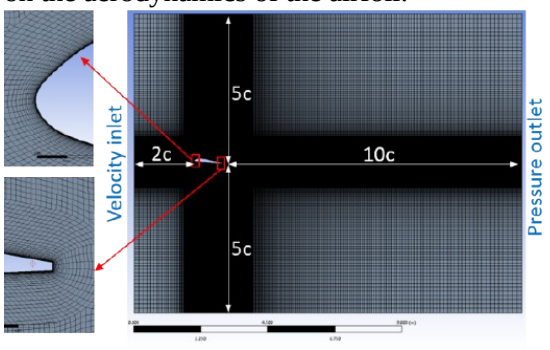

Fig. 3. The Computational domain and generated mesh for out-of-ground effect validation

A structured multi-block mesh was applied with exception to the area around the airfoil which is a quadrilateral dominant mesh. Bias was applied to ensure a smooth transition. The inflation mesh was applied around the airfoil and refined into a viscous sublayer to maintain the first layer non-dimensional height ($y+$) of approximately 1 which is suitable for the SST k-ω turbulence model. The first layer thickness is approximately 4×10^{-6} of the chord length.

The meshes were refined with an increased number of elements until the changes in C_l, C_d and C_m were insignificant while keeping the maximum $y+$ around 1. The results became independent of mesh density when the number of elements reached about 420,000 as shown in Fig. 4. The meshing procedure was applied further in other simulations in this study.

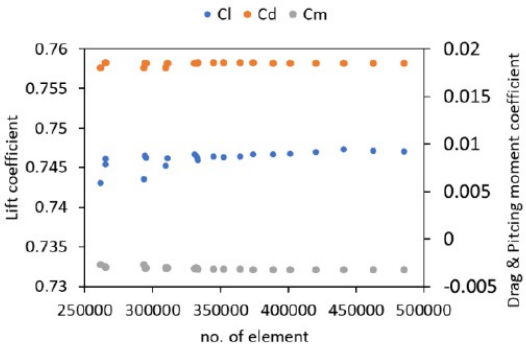

Fig. 4. Result of mesh independence study for N60R at *Re* of 3×10^6, *Ma* = 0.13 and $\alpha = 6°$

3.3 Model validation

Prior to the investigation of the aerodynamic characteristics of the N60R airfoil in GE, the computational method was validated against the experimental and theoretical data of the airfoil operated in the free stream from NACA Technical Note no.388 (TN 388) and the JavaFoil application, developed by Martin Hepperle [22]. The JavaFoil algorithms are based on the procedures described by Richard Eppler et al. [23-25]. The calculations were done with the airfoil located out of ground effect at an average flow velocity 45 m/s, *Re* of 3×10^6 and *Ma* = 0.13. The results are shown in Fig. 5.

A good agreement of lift is achieved with JavaFoil but was overpredicted compared with TN 388. Drag prediction is higher than both JavaFoil and TN 388. The pitching moment concurred with TN 388 and was better than

JavaFoil. The center of pressure location is accurately predicted. Since the SST *k-ω* model assumes a fully turbulent flow, it causes an overestimation of turbulence in regions with high normal strain, such as stagnation and strong acceleration. It creates high momentum transfers near the wall which delay the flow separation [26]. This may result in an over-prediction of the lift and drag.

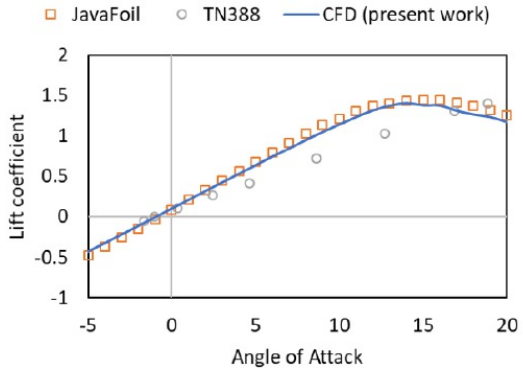

(a) Lift coefficient

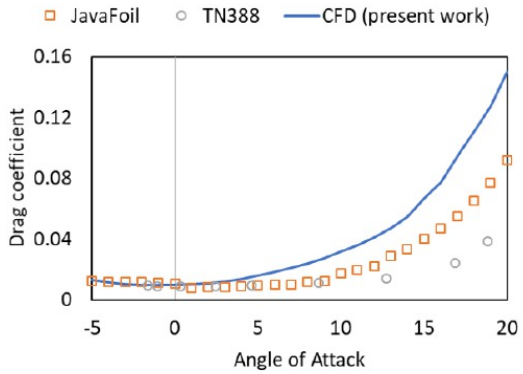

(b) Drag coefficient

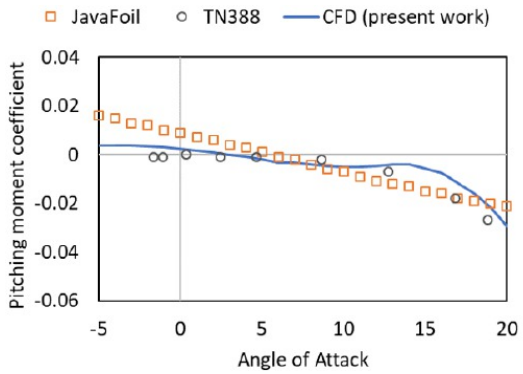

(c) Pitching moment coefficient

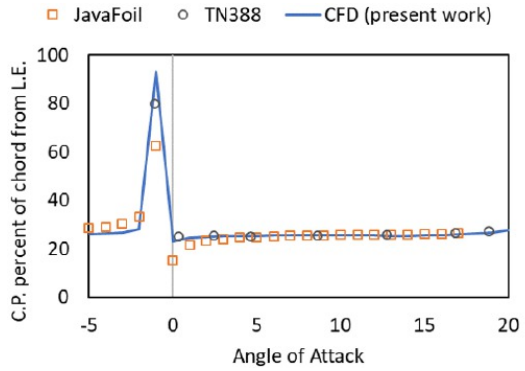

(d) Center of pressure percent of chord from leading edge

Fig. 5. Aerodynamic characteristics of N60R in free stream

4. Computational domain and flow conditions

The numerical analysis of the N60R operating in ground effect is set up similar to the free stream flight validation in section 3.3, except the height of the trailing edge is defined as h_t. The angle of attack range is 0°-20°. Various flow velocities and corresponding *Re* were set up as shown in Table 1. The ground clearance ratio (h_c) was varied from 0.05, 0.1, 0.15, 0.2, 0.25, 0.3, 0.5, 0.75, 1, 1.25 and 1.5.

Table 1
Flow velocity and the corresponding *Re* (based on the chord)

Flow velocity (m/s)	*Re* (× 10^6)
12	0.8
15	1
30	2
45	3
60	4
75	5

According to Table 1, the range of *Ma* is between 0.03 and 0.22, thus the flow is incompressible. A pressure-based coupled algorithm was applied with double-precision solvers. The governing equations were discretized with the second-order upwind method. The computational domain and the generated mesh, with h_c = 0.3, are shown in Fig. 6.

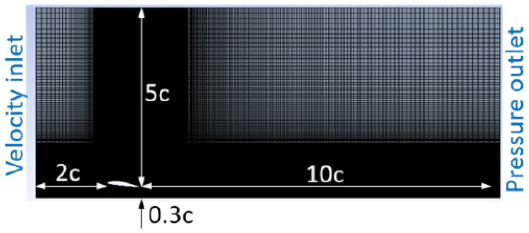

Fig. 6. Computational domain and mesh of N60R at h_c = 0.3

5. Results and discussion

5.1 Pressure and velocity distributions

Figure 7-8 show the pressure contour for a flow velocity of 75 m/s at h_c = 0.3 and 0.05, respectively. High pressure is located under the airfoil near the leading edge then decreases as the distance from the leading edge increases while the suction-lift occurs on the upper surface. At very low h_c (Fig. 8), high pressure builds up along the chord length due to the ramming effect.

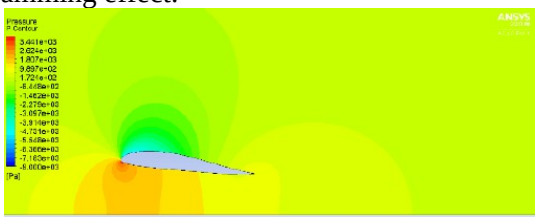

(a) α = 6°

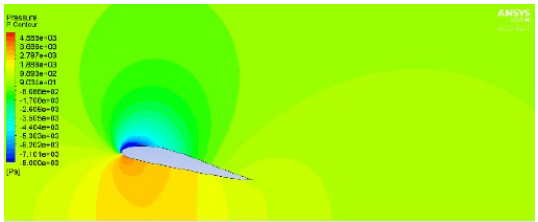

(b) α = 12°

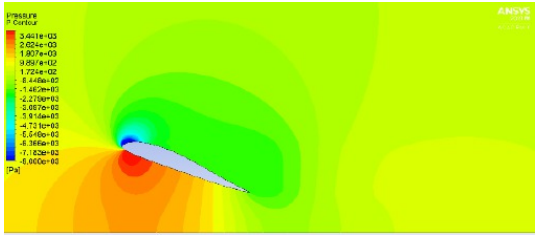

(c) α = 20°

Fig. 7. Pressure contour for a flow velocity of 75 m/s at h_c = 0.3

(a) α = 6°

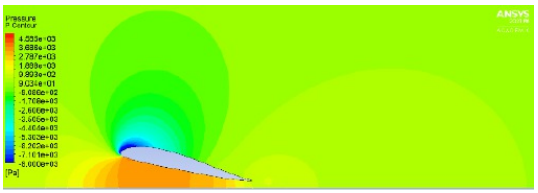

(b) α = 12°

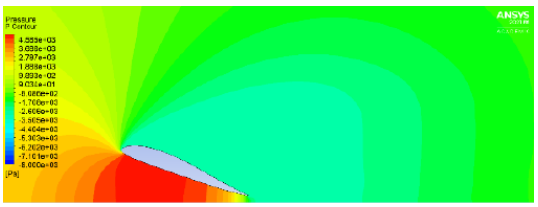

(c) α = 20°

Fig. 8. Pressure contour for a flow velocity of 75 m/s at h_c = 0.05

The pressure distribution at α = 6°, 12° and 20° at h_c = 0.3 and 0.05 is shown in Fig. 9. Interestingly, the upper surface loses the suction-lift at small α. At α less than the stall angle, the difference of the pressure over the airfoil is insignificant for both h_c = 0.3 and 0.05 (Fig. 9(a)-9(b)).

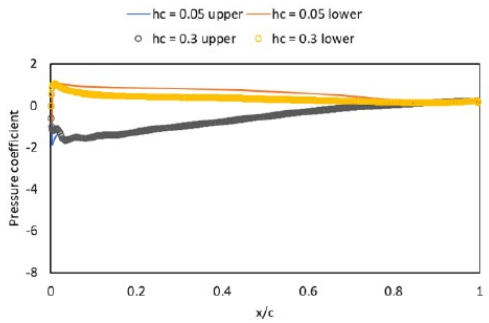

(a) α = 6°

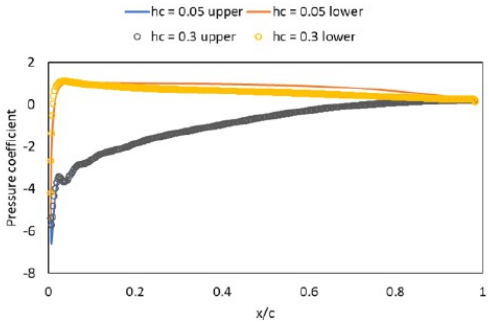

(b) α = 12°

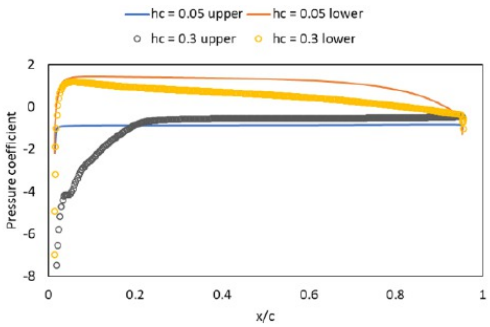

(c) $\alpha = 20°$

Fig. 9. Pressure coefficient distribution

The velocity contours in Fig. 10-11 show that as h_c decreases, the trailing edge, which is close to the ground, traps the air underneath. Hence more air flows over the upper surface, lowering the pressure over the upper surface of the airfoil. This low pressure creates suction-lift while the air underneath slows down and near-stagnation pressure occurs. Both suction-lift on the upper surface and high pressure on the lower surface create a significant increase in C_l.

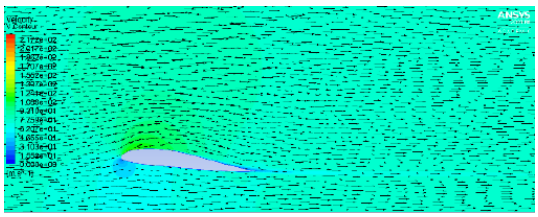

(a) $\alpha = 6°$

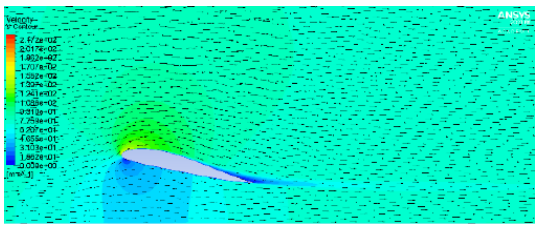

(b) $\alpha = 12°$

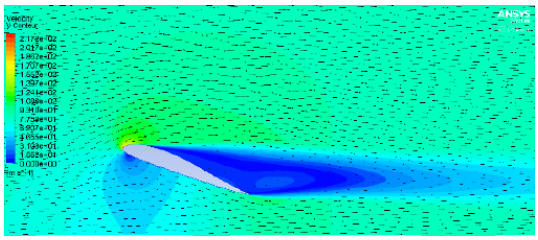

(c) $\alpha = 20°$

Fig. 10. Velocity contour and vector for a flow velocity of 75 m/s at $h_c = 0.3$

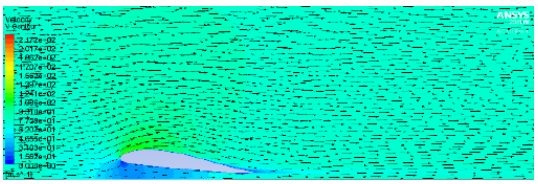

(a) $\alpha = 6°$

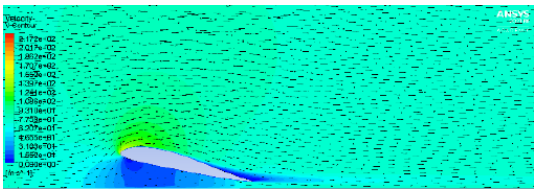

(b) $\alpha = 12°$

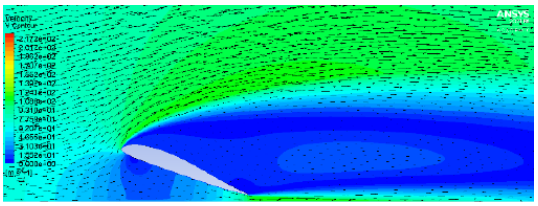

(c) $\alpha = 20°$

Fig. 11. Velocity contour and vector for a flow velocity of 75 m/s at $h_c = 0.05$

When α approaches stall angle (~12°), flow separation occurs on the upper surface close to the trailing edge. The separation is more severe and occurs at lower α with the decrease in h_c.

5.2 Aerodynamic characteristics

Lift curves for various h_c at flow velocity 12 and 75 m/s are shown in Fig. 12. The lift curve for $h_c \geq 0.5$ exhibits a linear portion when $0° < \alpha < 12°$ but shows curvature at low h_c. Lower h_c exhibits greater curvature. Fig. 13 shows C_l versus h_c at the same velocity. The change of C_l is insignificant for $h_c \geq 0.5$. However, for $h_c \leq 0.3$ and $\alpha \geq 3$, C_l increases significantly as h_c decreases. An incidence of zero lift becomes less negative or becomes positive as h_c decreases. The same behavior occurs on flow velocities ranging from 12 to 75 m/s (Re from 0.8 to 5×10^6).

C_d increases as α increases, especially when $\alpha > 12°$ when the separation occurs. However, C_d increases sharply at very low h_c due to the flow congestion in the passage between the airfoil and ground as shown in Fig. 14. The change of C_d is also insignificant for $h_c \geq 0.5$, as shown in Fig. 15.

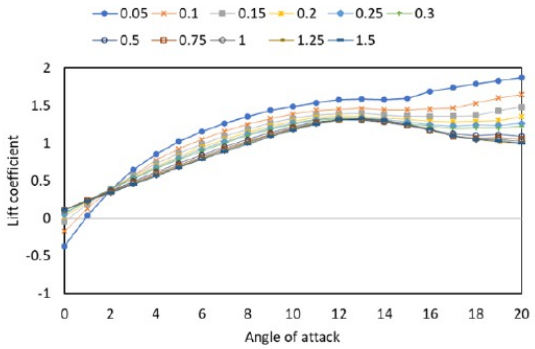

(a) 12 m/s

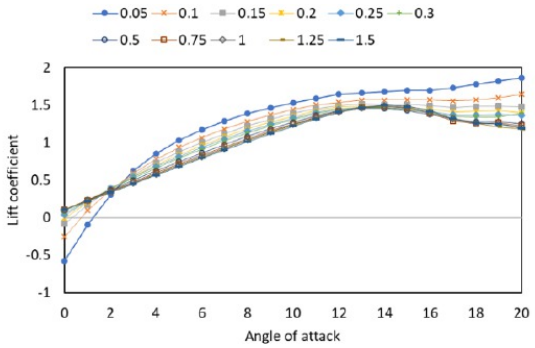

(b) 75 m/s

Fig. 12. Lift coefficients for various h_c at flow velocity 12 and 75 m/s

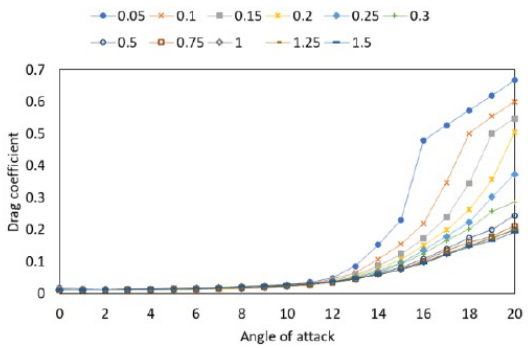

(a) 12 m/s

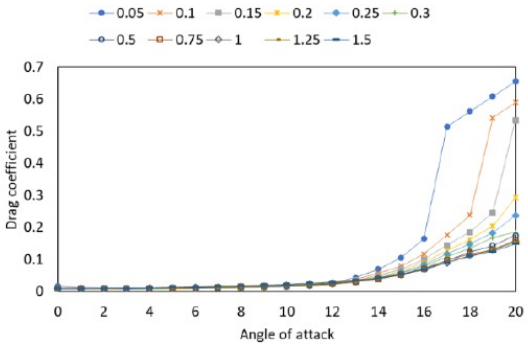

(b) 75 m/s

Fig. 14. Drag coefficients for various h_c at flow velocity 12 and 75 m/s

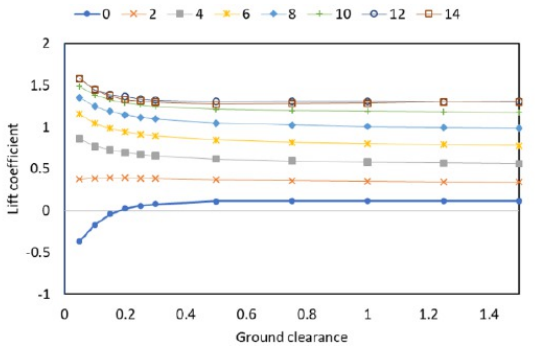

(a) 12 m/s

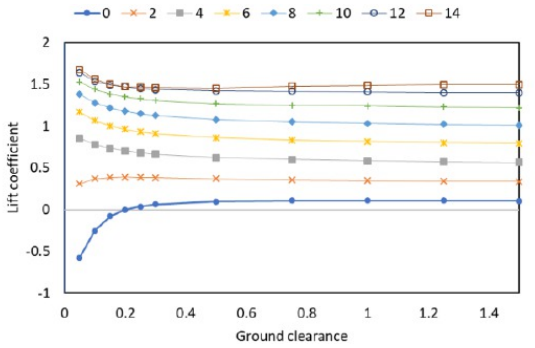

(b) 75 m/s

Fig. 13. Lift coefficients versus h_c at flow velocity 12 and 75 m/s

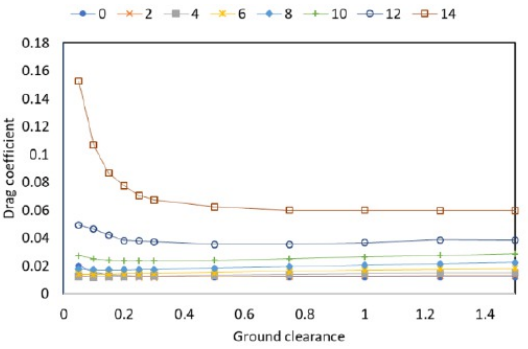

(a) 12 m/s

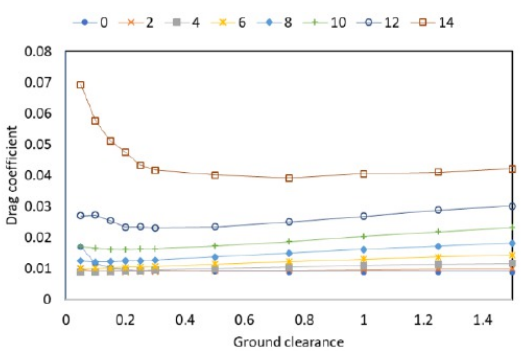

(b) 75 m/s

Fig. 15. Drag coefficients versus h_c at flow velocity 12 and 75 m/s

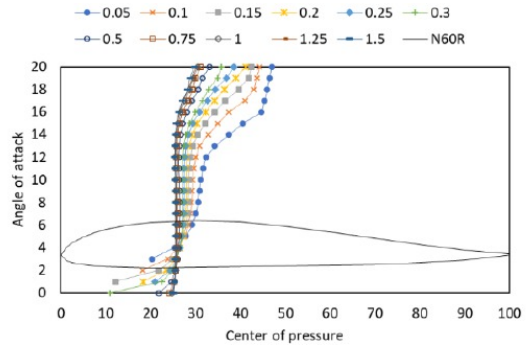

(a) 12 m/s

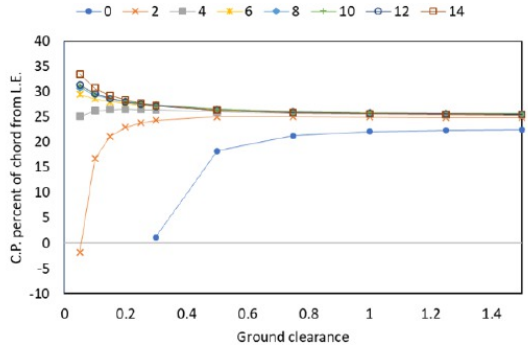

(b) 75 m/s

Fig. 16. Center of pressure (percent of chord from the leading edge) for various h_c at flow velocity 12 and 75 m/s

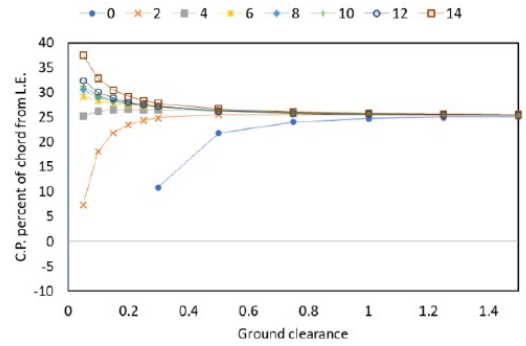

(a) 12 m/s

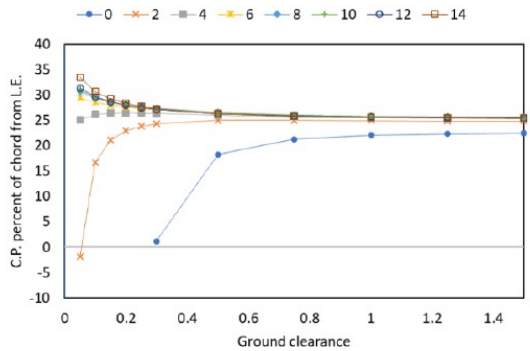

(b) 75 m/s

Fig. 17. Center of pressure (percent of chord from the leading edge) for various α versus h_c at flow velocity 12 and 75 m/s

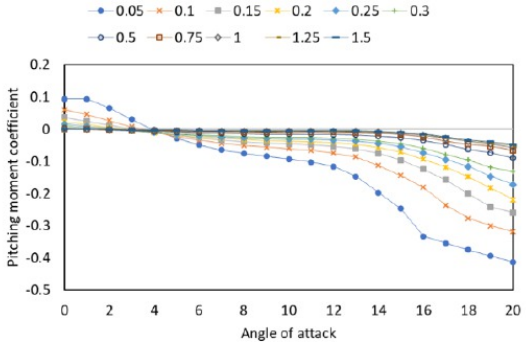

(a) 12 m/s

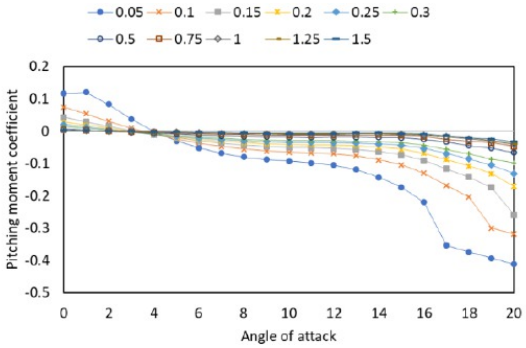

(b) 75 m/s

Fig. 18. Pitching moment coefficients for various h_c at flow velocity 12 and 75 m/s

In Fig. 16-17, for $h_c \geq 0.5$, the location of X_{cp} is approximately a quarter of the chord from the leading edge similar to flight in free stream over the useful angle of attack before stall. In contrast to in-ground-effect flight ($h_c < 0.5$), the center of pressure shifts further to the trailing edge. The center of pressure may move to nearly half chord position especially at high α and when the airfoil is extremely closed to the ground.

By convention, the pitching moment is defined as negative when it acts to pitch the airfoil in the nose-down direction. From Fig. 18, for $h_c \geq 0.5$, C_m is practically constant and close to zero over the useful range of α up to the stall angle, and the negative moment slightly increases after stall. For $h_c \leq 0.3$, the negative moment is significantly increased by h_c since X_{cp} moves further away from the leading edge (Fig. 19).

The effect of h_c on lift-to-drag ratio is demonstrated in Fig. 20-21. The increase in

lift-to-drag ratio is clearly seen as the airfoil is close to the ground (h_c < 0.5).

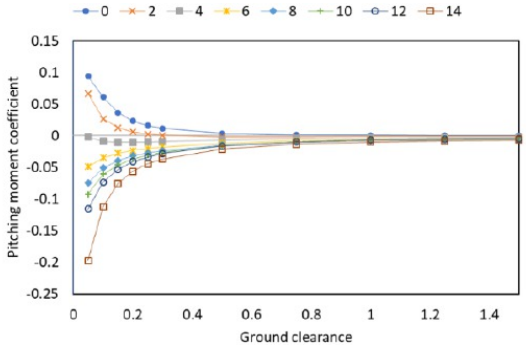

(a) 12 m/s

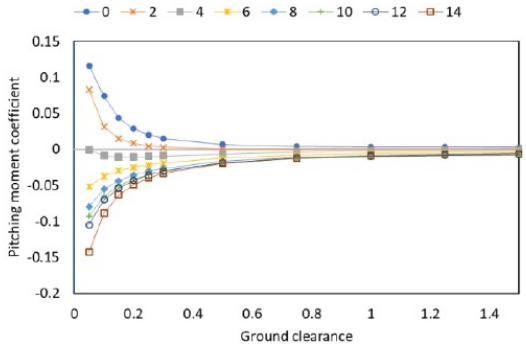

(b) 75 m/s

Fig. 19. Pitching moment coefficients versus h_c at flow velocity 12 and 75 m/s

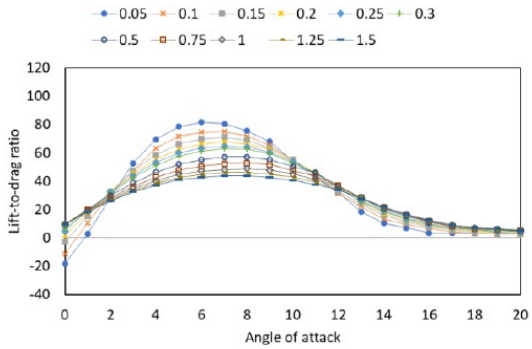

(a) 12 m/s

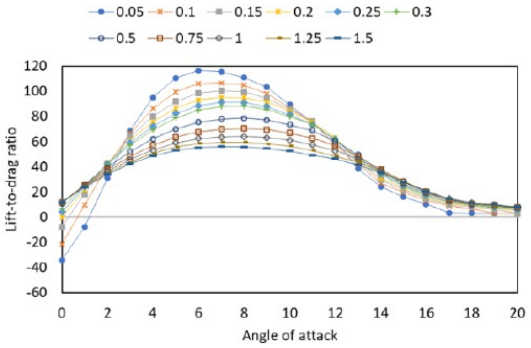

(b) 75 m/s

Fig. 20. Lift-to-drag ratio for various h_c at flow velocity 12 and 75 m/s

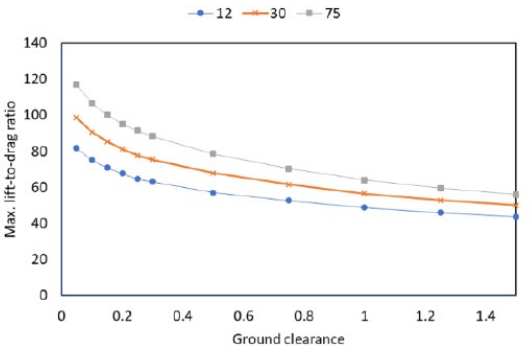

Fig. 21. Maximum lift-to-drag ratio versus h_c for various flow velocity

To maximize efficiency, the WIG craft should cruise at a medium angle of attack ($2°<\alpha<12°$) to obtain high lift-to-drag ratio and maintain h_c > 0.15 to avoid instability at low ground clearance.

5.3 Regression models

There are some difficulties in performing a numerical study of the airfoil operating in GE. First, the mesh must be regenerated for each h_c and α, which is a time-consuming process. Second, a large number of cells are required in the vicinity of the ground to capture the high-pressure gradient. To maximize utilization of generated data from numerical studies, the relationship between a set of variables (α, h_c and flow velocity) and the response variables (aerodynamic characteristics such as C_l, C_d and C_m) can be described using regression analysis.

Over the useful range of α (0°-15°), the Analysis of Variance (ANOVA) with the significant level 0.05 has been analyzed. The value of α, h_c and flow velocity are defined as

factors *A*, *B* and *C* respectively. The result of ANOVA for C_l is summarized in Table 2 with R^2= 99.56%.

The regression model can be written as:

$$y = \beta_0 + \beta_1 A + \beta_2 B + \beta_3 C + \beta_4 AA + \beta_5 BB + \beta_6 CC + \beta_7 AB + \beta_8 AC + \beta_9 BC + \beta_{10} ABC \quad (13)$$

Table 2
ANOVA result of C_l

Source	DOF	Adjusted sums of squares	F-value	P-value
Model	10	231.734	3600.41	0.000
A	1	37.466	5821.09	0.000
B	1	0.462	71.73	0.000
C	1	0.000	0.06	0.803
AA	1	16.579	2575.91	0.000
BB	1	0.676	105.00	0.000
CC	1	0.025	3.93	0.048
AB	1	0.146	22.75	0.000
AC	1	0.195	30.36	0.000
BC	1	0.001	0.10	0.753
ABC	1	0.001	0.10	0.756
Error	1045	6.726		
Total	1055	238.46		

where y is the response (such as C_l), β_i (for i = 0,1,..,10) are constants whose values are to be determined, *A* is a variable that represents α, *B* represents h_c and *C* represents the flow velocity. *AB*, *AC*, *BC* and *ABC* represent the interaction between *A* and *B*, *A* and *C*, *B* and *C*, *A* and *B* and *C* respectively.

From Table 2, the P-value for *C*, *BC* and *ABC* are greater than 0.05, indicating they are not statistically significant. However, the term *CC* and the interaction *AC* are significant (P-value < 0.05), thus factor *C* cannot be excluded from the model. The same procedure was conducted for C_l, C_d, C_m and lift-to-drag ratio. The constants β_i for all responses after removing insignificant factors are summarized in Table 3.

Table 3
Constants of the regression models

β_i	C_l	C_d	C_m	*L/D*
0	0.0610	0.01550	0.03429	1.41
1	0.19385	-0.002260	-0.012457	17.052
2	-0.2379	-0.00618	0.01864	-17.70
3	0.000226	-0.000119	-	0.4459
4	-0.006632	0.000548	0.000220	-1.1493
5	0.1464	0.01176	-0.03566	3.36
6	-0.000012	0.000003	-	-0.003345
7	-0.01002	-0.002275	0.007717	0.176
8	0.000204	-0.000045	-	0.01387
9	-	-0.000107	-	-
10	-	0.000026	-	-

The R^2 of the models representing C_l, C_d and C_m and lift-to-drag ratio after removing insignificant terms are 99.56%, 97.36%, 91.31% and 94.04%, respectively. The response surfaces for the predicted C_l, C_d and C_m and lift-to-drag ratio at flow velocity 75 m/s can be generated as shown in Fig. 22-25.

It is shown that C_l increases as α increases and h_c decreases while minimum C_d occurs: around α = 4° to 6° when h_c is less than 0.8. The maximum lift-to-drag ratio is located around α = 6° to 8° and decreases as h_c increases.

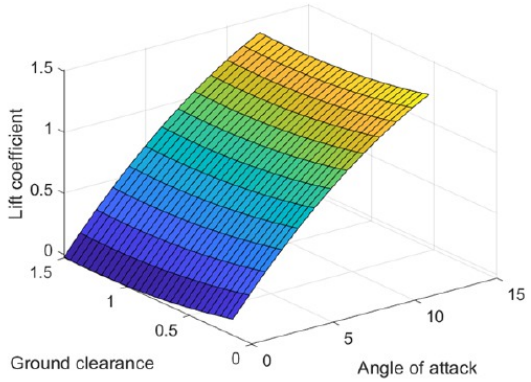

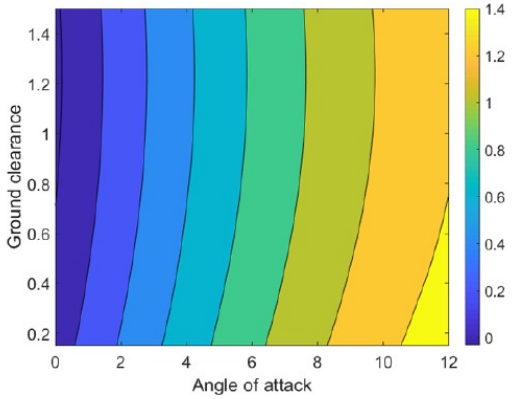

Fig. 22. Response surface and the contour of the predicted C_l

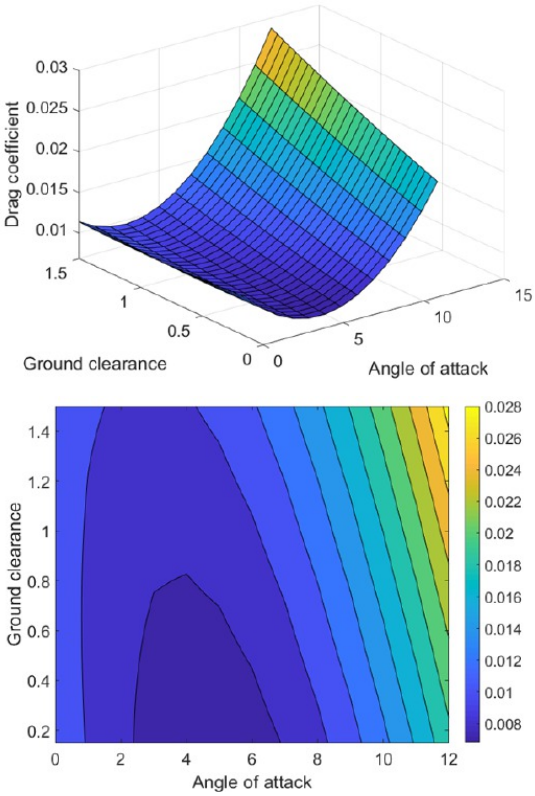

Fig. 23. Response surface and the contour of the predicted C_d

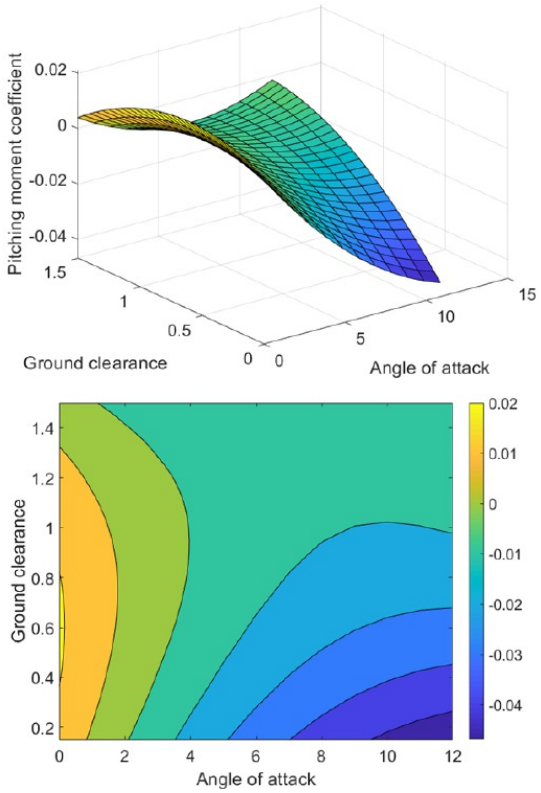

Fig. 24. Response surface and the contour of the predicted C_m

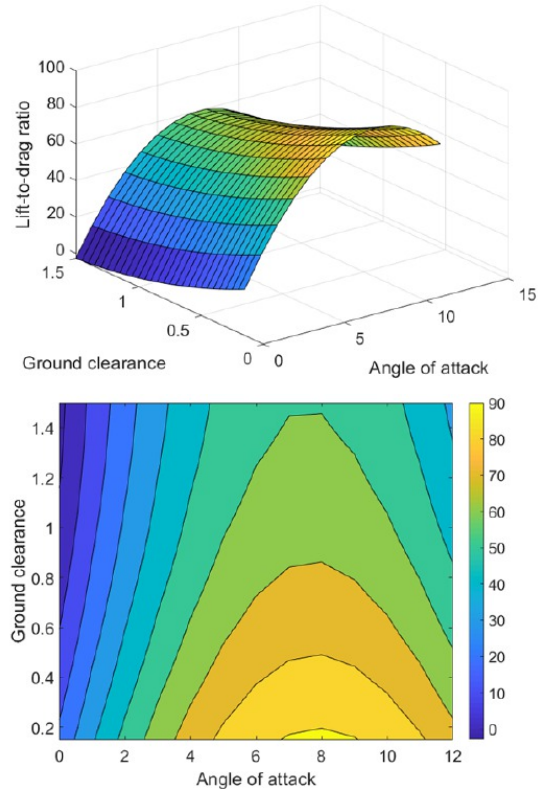

Fig. 25. Response surface and the contour of the predicted lift-to-drag ratio

5.3 Backtesting of the regression models

To validate the accuracy and performance of the models described in the previous section, a comparison between data from CFD and regression was conducted. The results at flow velocity 75 m/s are shown in Fig. 26. The regression accuracy is acceptable in the range of α (2° to 12°). The lift is predicted quite well except at h_c = 0.15, which is under-predicted. The drag is under-predicted for all ranges of α and h_c. The error of the moment coefficient prediction is quite large for h_c = 0.15 but acceptable for h_c > 0.3.

6. Conclusions

A numerical study of the reflexed airfoil, N60R, was conducted to investigate the effect of α, h_c and flow velocity on the aerodynamic characteristics in GE. It is clearly shown that the GE has an effect on C_l, C_d, C_m, and X_{cp}, especially when h_c< 0.5. The pitching moment is almost equal to zero over a useful range of α but the nose-down moment increases as h_c decreases below 0.3. At an angle of attack approximately 6° to 7°, the maximum lift-to-drag ratio can be achieved. The increase in the lift-to-drag ratio enhances the efficiency of the airfoil compared with the out-of-ground effect flight.

The regression models were presented to predict the C_l, C_d, C_m and lift-to-drag ratio with acceptable accuracy for α ranging from 2° to 12° and h_c from 0.15 to 1.5.

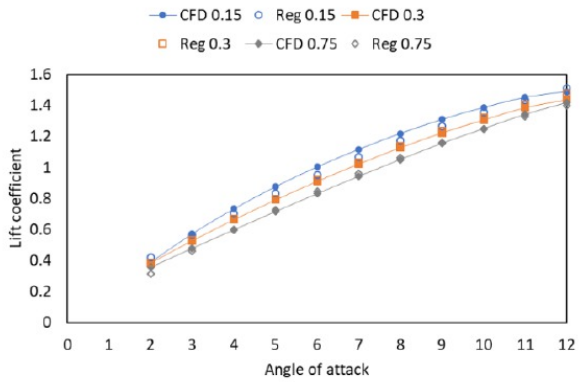

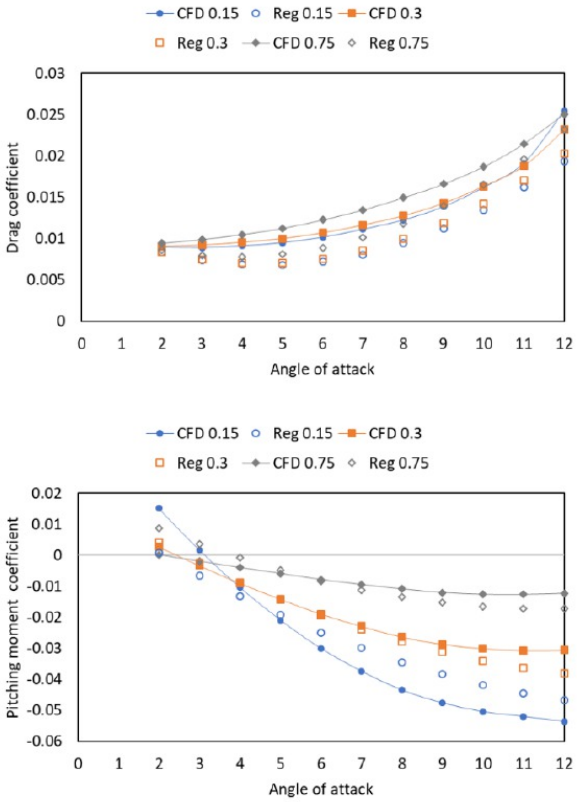

Fig. 26. Comparison between data from CFD and the regression

Acknowledgement

The author would like to thank CADFEM SEA Pte. Ltd. - A certified Elite Channel Partner to ANSYS - for providing support and access to the CFD program named ANSYS Fluent 2021 R1.

References

[1] G. Gabrielli and T. von Kármán, "What price speed? Specific power required for propulsion of vehicles," *Mechanical Engineering, ASME*, 72(10) (1950) 775-781.

[2] N. V. Kornev and K. Matveev, "Complex Numerical Modeling of Dynamics and Crashes of Wing-in-Ground Vehicles," *41st Aerospace Sciences Meeting and Exhibit*, 2003.

[3] K. Park and J. Lee, "Influence of endplate on aerodynamic characteristics of low-aspect-ratio wing in ground effect," *Journal of Mechanical Science and Technology*, 22(12) (2008) 2578-2589.

[4] M. Halloran and S. O'Meara, "Wing in

Ground Effect Craft Review," The Sir Lawrence Wackett Centre for Aerospace Design Technology, Royal Melbourne Institute of Technology, Melbourne, Australia, 1999.

[5] R. Ranzenbach and J. Barlow, "Cambered Airfoil in Ground Effect - An Experimental and Computational Study," *SAE Technical Paper 960909*, 1996.

[6] H. H. Chun and C. H. Chang, "Turbulence flow simulation for wings in ground effect with two ground conditions: fixed and moving ground," *International Journal of Maritime Engineering*, 145(A3) (2003) 1-18.

[7] M. R. Ahmed, T. Takasaki, and Y. Kohama, "Aerodynamics of a NACA4412 Airfoil in Ground Effect," AIAA, 2007.

[8] Y.-S. Kim, J.-E. Lee, E.-G. Kim, and J.-H. Kwon, "Turbulent Flow Simulations on 2-Dimensional Ground Effect Part II. Study on the Effects of Ground Boundary Conditions," *Journal of Korean Society for Aeronautical & Space Sciences*, 35(8) (2007) 670-676.

[9] K. H. Jung, H. H. Chun, and H. J. Kim, "Experimental investigation of wing-in-ground effect with a NACA6409 section," *Journal of Marine Science and Technology*, 13(4) (2008) 317-327.

[10] X. Qin, P. Liu, and Q. Qu, "Aerodynamics of a Multi-Element Airfoil near Ground," *Tsinghua Science & Technology*, 14 (2009) 94-99.

[11] W. Yang and Z. Yang, "Aerodynamic Investigation of a 2D Wing and Flows in Ground Effect," *Chinese Journal of Computational Physics*, 2009.

[12] M. R. Ahmed and S. D. Sharma, "An investigation on the aerodynamics of a symmetrical airfoil in ground effect," *Experimental Thermal and Fluid Science*, 2005.

[13] W. Yang and Z. Yang, "Effects of Design Parameters on Longitudinal Static Stability for WIG Craft," *International Journal of Aerodynamics*, 2010.

[14] W. Yang, C.-J. Ying, and Z.-g. Yang, "Aerodynamic study of WIG craft near curved ground," *Journal of Hydrodynamics*, 22(5) (2010) 371-376.

[15] Q. Qu, X. Jia, W. Wang, R. K. Agarwal, and P. Liu, "Aerodynamics and Flow Physics of a NACA 4412 Airfoil in Dynamic Ground Effect," AIAA, 2014.

[16] M. Tahani, M. Masdari, and A. Bargestan, "Aerodynamic performance improvement of WIG aircraft," *Aircraft Engineering and Aerospace Technology*, 2017.

[17] A. E. Ockfen and K. I. Matveev, "Aerodynamic characteristics of NACA 4412 airfoil section with flap in extreme ground effect," *International Journal of Naval Architecture and Ocean Engineering*, 2009.

[18] D. P. Raymer, Aircraft Design: A Conceptual Approach. American Institute of Aeronautics and Astronautics, Incorporated, 2018.

[19] F. R. Menter, "Two-equation eddy-viscosity turbulence models for engineering applications," AIAA, 1994.

[20] ANSYS, ANSYS Fluent Theory Guide. ANSYS, Inc., 2013.

[21] G. L. Defoe, "A Comparison of the Aerodynamic Characteristics of Three Normal and Three Reflexed Airfoils in the Variable Density Wind Tunnel," Langley Memorial Aeronautical Laboratory, 1931.

[22] M. Hepperle. "JavaFoil." https://www.mh-aerotools.de/airfoils/javafoil.htm [accessed 01.04.2020].

[23] R. Eppler, "Praktische Berechnung laminarer und turbulenter Absauge-Grenzschichten," *Ingenieur-Archiv*, 32(4) (1963) 221-245.

[24] R. Eppler, "Turbulent Airfoils for General Aviation," *Journal of Aircraft*, 15(2) (1978) 93-99.

[25] R. Eppler and D. M. Somers, "A computer program for the design and analysis of low-speed airfoils," NASA Langley Research Center; Hampton, VA, United States, 1980.

[26] T. Chitsomboon and C. Thamthae, "Adjustment of k-ω SST Turbulence Model for an Improved Prediction of Stalls on Wind Turbine Blades," *Proceeding of World Renewable Energy Congress*, 2011.